Chinese Chemical Letters 37 (2026) 111799

Contents lists available at ScienceDirect

Chinese Chemical Letters

journal homepage: www.elsevier.com/locate/cclet

Ultra-low-dose radioimmunotherapy improves prostate cancer treatment efficacy and safety

Hong Wang[a,1], Zhenwen Zhao[a,1], Xiao Xu[b,c,*], Zhide Guo[a,*], Gang Liu[a,*]

[a] State Key Laboratory of Vaccines for Infectious Diseases, Center for Molecular Imaging and Translational Medicine, Xiang An Biomedicine Laboratory, National Innovation Platform for Industry-Education Integration in Vaccine Research, School of Public Health, Xiamen University, Xiamen 361102, China
[b] Cancer Center, Dongguan Engineering Research Center for Innovative Boron Drugs and Novel Radioimmune Drugs, The Tenth Affiliated Hospital, Southern Medical University (Dongguan People's Hospital), Southern Medical University, Dongguan 523059, China
[c] Guangdong Engineering Research Center of Boron Neutron Therapy and Application in Malignant Tumors, The Tenth Affiliated Hospital, Southern Medical University (Dongguan People's Hospital), Southern Medical University, Dongguan 523059, China

ARTICLE INFO

Article history:
Received 17 December 2024
Revised 5 September 2025
Accepted 7 September 2025
Available online 8 September 2025

Keywords:
PSMA
GRPR
Theranostics
Tumor heterogeneity
Ultra-low-dose radioimmunotherapy

ABSTRACT

Prostate cancer poses a severe threat to the health of middle-aged and elderly males. In recent years, the development and clinical utilization of prostate-specific membrane antigen (PSMA)-targeted agents have significantly expanded diagnostic options for this malignancy. However, tumor heterogeneity substantially compromises the efficacy of radionuclide therapy, necessitating the exploration of multi-target strategies as potential solutions. This study presents a novel heterodimeric construct engineered for prostate cancer management, labeled with both diagnostic and therapeutic radionuclides to enable concurrent application in positron emission computed tomography (PET) imaging and radionuclide therapy. Our investigation primarily evaluates the therapeutic efficacy of ultra-low-dose (3.7 MBq) radionuclide therapy combined with anti-programmed cell death protein-1 (PD-1) antibody immunotherapy. In the RM-1 prostate cancer model with elevated PSMA expression, we have validated that the combination of ultra-low-dose radionuclide treatment and anti-PD-1 antibody immunotherapy yields superior therapeutic outcomes. Notably, compared to the immunotherapy-only group, the combination regimen elicited a significant increase in dendritic cells (DCs) and natural killer (NK) cells populations, with enhancements ranging from 32 % to 103 %. This ultra-low-dose radioimmunotherapy strategy offers a valuable theoretical framework for clinical translation, holding promise for further enhancing therapeutic efficacy in prostate cancer treatment.

© 2026 Published by Elsevier B.V. on behalf of Chinese Chemical Society and Institute of Materia Medica, Chinese Academy of Medical Sciences.

According to projections by the American Cancer Society (ACS), the United States is expected to see over 2 million new cancer cases in 2024, with >610,000 cancer-related deaths. Notably, prostate cancer is anticipated to account for a significant portion of these cases, with an estimated incidence of nearly 299,000, representing 29 % of all male cancer cases. It is also the most prevalent cancer among males in terms of incidence. Furthermore, approximately 35,250 male patients are predicted to succumb to prostate cancer, resulting in an 11 % mortality rate, making it the second leading cause of cancer-related deaths after lung cancer. Importantly, the incidence of prostate cancer has increased by 3 % annually between 2014 and 2019, leading to an additional 99,000 cases compared to periods of stable rates. Alarmingly, nearly half of these cases were diagnosed at advanced stages [1–3].

Historically, prostate cancer detection relied on prostate-specific antigen concentration, transrectal prostate biopsy, and multiparametric magnetic resonance imaging. However, these methods had limitations such as inadequate specificity and potential infection risks [4–7]. The identification of prostate-specific membrane antigen (PSMA), also known as glutamate carboxypeptidase, in extracts of the LNCaP cell line [8]. Studies have shown that PSMA is highly expressed in prostate tumor cells, with significantly lower levels in normal tissues, ranging from one thousandth to one-hundredth of that in tumor cells [9]. Recent advancements in radiopharmaceuticals targeting PSMA have greatly improved the diagnosis and treatment of prostate cancer. PSMA expression is closely correlated with cancer progression, metastasis, and recurrence, and is significantly upregulated in castration-resistant prostate cancer. The increased utilization of glutamine by prostate tumor cells suggests a reliance on PSMA for nucleotide biosynthesis and metabolism,

* Corresponding authors.
E-mail addresses: xiaoxu721@smu.edu.cn (X. Xu), gzd666888@xmu.edu.cn (Z. Guo), gangliu.cmitm@xmu.edu.cn (G. Liu).
[1] These authors contributed equally to this work.

https://doi.org/10.1016/j.cclet.2025.111799
1001-8417/© 2026 Published by Elsevier B.V. on behalf of Chinese Chemical Society and Institute of Materia Medica, Chinese Academy of Medical Sciences.

impacting cell proliferation and invasion [10]. Diagnostic drugs targeting PSMA, such as [^{68}Ga]Ga-PSMA-11 and [^{177}Lu]Lu-PSMA-617, have been introduced into clinical practice, offering more treatment options for patients with castration-resistant prostate cancer [11].

The G protein-coupled receptor (GRPR) is significantly expressed in prostate cancer and overexpressed in various other cancer types, including breast, ovarian, lung, colon, esophageal, and gliomas. Molecules targeting GRPR hold promise as versatile tumor molecular probes with broad applicability [12–17]. Recent advancements in the development of radioligands targeting GRPR, using both agonist- and antagonist-based approaches, have shown promising results. Antagonists, in particular, have demonstrated reduced off-target effects, improved pharmacokinetic properties, and enhanced tumor uptake compared to agonists, resulting in higher tumor-to-background ratios [18–20]. Preclinical studies on probes like [^{68}Ga]Ga-RM2 and [^{111}In]In-RM2 have further highlighted their potential [21,22].

Radioactive molecular probes targeting a single receptor, such as PSMA or GRPR, have shown promise in diagnosing and treating prostate cancer and other malignancies. However, the tumor microenvironment's complexity and heterogeneity often limit the effectiveness of single-target diagnostics and treatments. Given the upregulation of both PSMA and GRPR in prostate cancer, combining these targets may have synergistic effects [23–25]. It is crucial to consider the side effects of current nuclide-only therapies [26,27]. A clinical study in Germany using [^{177}Lu]Lu-PSMA-617 reported long-term nephrotoxicity and high uptake in the salivary and lacrimal glands, leading to dry mouth and reduced quality of life, and necessitating treatment discontinuation [28–31]. High-dose radiotherapy significantly elevates the risk of acute and late toxic reactions. Meta-analysis of radiotherapy data for prostate cancer reveals that 92.5% of patients receiving high-dose radionuclide therapy developed acute radiogenic toxicity, while 100% of subjects experienced late radiation-induced injury. With regard to the toxicity spectrum, genitourinary and gastrointestinal toxicities constitute the predominant types of acute and long-term complications. Acute manifestations are characteristically marked by lower urinary tract irritative symptoms (*e.g.*, pollakiuria, urinary urgency, hematuria) and proctitis, whereas late complications predominantly manifest as organic injuries such as bladder contracture and rectal stenosis [32–35]. Non-specific uptake in non-target organs or tissues can cause undesired side effects, hindering the progression of these therapies to phase III clinical trials and the market.

The advent of programmed death receptor-1/programmed death receptor ligand 1 (PD-1/PD-L1) inhibitors has ushered in a revitalization of immunotherapy, with their exceptional efficacy positioning them as the predominant immunosuppressants in clinical practice [36–38]. However, numerous studies have demonstrated that the efficacy of monotherapy with PD-1/PD-L1 inhibitors in solid tumors is constrained to a range of 20%–40% [39,40]. The combination of these inhibitors with radiation therapy has been shown to elicit favorable alterations within the tumor microenvironment, including augmented antigen exposure and enhanced antigen presentation. This, in turn, facilitates immune microenvironment remodeling and augments the potency of immunotherapy [41–43]. Nonetheless, high-dose radiation exerts a dual influence. While it effectively induces DNA double-strand breaks, leading to the destruction of tumor cells, it may also inadvertently damage immune cells residing within the tumor microenvironment [44–46]. This unintended consequence has the potential to impair radiation's ability to eliminate tumor cells and obstruct the activation of the immune system against the tumor.

In the current study, a rational design and synthesis approach was undertaken to develop a heterodimer targeting molecule, termed 1,4,7,10-tetraazacyclododecane-*N*,*N*',*N*,*N*'-tetraacetic acid (DOTA)-PSMA-GRPR. To assess the targeting and retention capabilities of this molecule, imaging studies were conducted using a mouse model bearing human prostate cancer PSMA(+) (PC3-PIP) tumors. Subsequently, both low-dose and high-dose radionuclide therapy experiments were performed in the same mouse model to evaluate therapeutic efficacy. Additionally, the efficacy and feasibility of combining ultra-low-dose radionuclide therapy with anti-PD-1 antibody immunotherapy were validated in a separate mouse model bearing RM-1^{PSMA+} tumors. Lastly, to ensure the safety and efficacy of this approach, immunohistochemical analysis was performed on the major organs and tissues of all treated animals. This comprehensive strategy aims to provide robust theoretical guidance and support for future clinical applications, paving the way for the translation of these findings into clinical practice.

The labeling precursor, DOTA-PSMA-GRPR (Fig. 1a), was synthesized following the procedure detailed in Supporting information. To enhance aqueous solubility, a polyethylene glycol (PEG) chain was intercalated between the two functional moieties. Lysine was used to adjust the spatial separation between the moieties. DOTA-*N*–hydroxy succinimide (NHS) was conjugated to lysine to facilitate chelation of the metal radionuclides ^{68}Ga and ^{177}Lu.

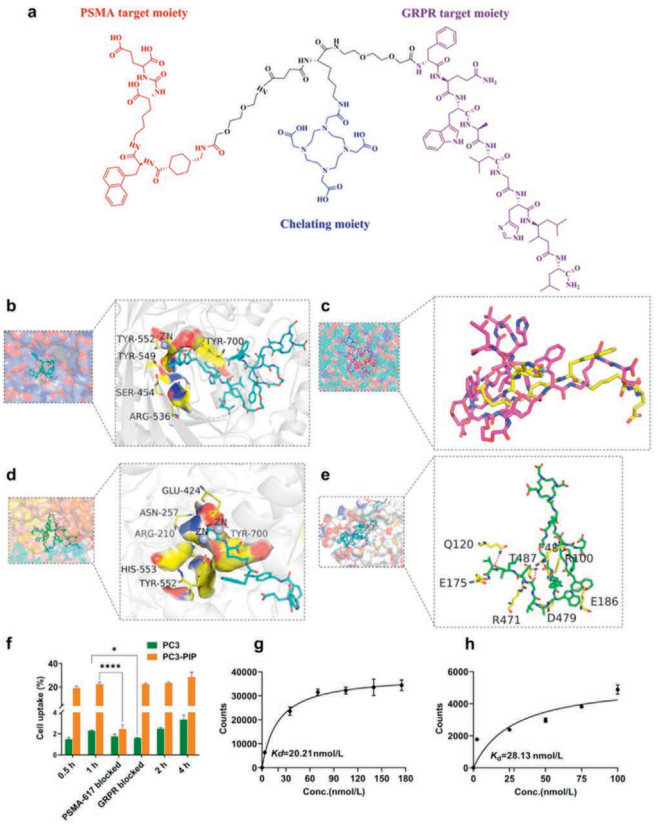


Fig. 1. Docking simulation calculations and cell experiments. (a) The molecular structure of DOTA-PSMA-GRPR. (b) The interaction between PSMA-1007 and the receptor protein revealing a significant polar interaction involving the EuK functional group and zinc ions. (c) Molecular docking demonstrates that DOTA-PSMA-GRPR and PSMA-1007 share a common binding pocket. (d) The interaction between DOTA-PSMA-GRPR and 5O5T showing polar interactions involving the EuK functional group and zinc ions. (e) The interaction between DOTA-PSMA-GRPR and the gastrin-releasing peptide receptor, revealing numerous polar interactions between DOTA-PSMA-GRPR and the amino acid residues in the protein. (f) Depicts the results of cellular uptake and blockade experiments. (g) The saturation binding for PC3-PIP cells is shown with a K_d value of 20.21 nmol/L. (h) The saturation binding for PC-3 cells is presented with a K_d value of 28.26 nmol/L. The data are presented as mean ± standard deviation (SD) ($n = 3$). $^{*}P < 0.05$, $^{****}P < 0.0001$.

The purity of DOTA-PSMA-GRPR was determined to be greater than 97 % (Fig. S6 in Supporting information). The retention time of free $^{68}GaCl_3$ and $^{177}LuCl_3$, as measured by radioactive high performance liquid chromatography (Radio-HPLC), was 4 min. The radiochemical yield, determined by Radio-HPLC and corrected for radioactive decay, was over 95 %. [^{68}Ga]Ga-DOTA-PSMA-GRPR demonstrated good stability in both phosphate buffered saline (PBS) and 10 % fetal bovine serum (FBS) (Fig. S7 in Supporting information). The radiochemical purity of [^{177}Lu]Lu-DOTA-PSMA-GRPR was assessed using both Radio-HPLC and Radio-thin-layer chromatography (TLC) methods. The results from Radio-TLC were consistent with those from Radio-HPLC, confirming a radiochemical purity exceeding 95 % for this probe (Fig. S8 in Supporting information). The stability of [^{177}Lu]Lu-DOTA-PSMA-GRPR was assessed at various time points using Radio-TLC. Even after 72 h of incubation in PBS and 10 % FBS, the radiochemical purity remained above 95 % (Figs. S9a and b in Supporting information), indicating good stability. The Log *P* value of [^{68}Ga]Ga-DOTA-PSMA-GRPR, determined using the lipid-water partition coefficient test, was -1.28 ± 0.09 ($n = 6$) (Table S2 in Supporting information), indicated the incorporation of GRPR marginally decreased its hydrophilicity in comparison to [^{68}Ga]/[^{177}Lu]-PSMA-617 (-1.28 *vs.* -2.00) [47], potentially impacting its pharmacokinetic properties.

In molecular docking simulation calculations [48], the ligand molecule PSMA-1007, within the crystal structure designated as 5O5T, establishes extensive polar interactions with the receptor protein. Specifically, the Glu-Urea-Lys functional group of PSMA-1007 exhibits significant polar interactions with zinc ions (Fig. 1b). This interaction pattern is also observed in the DOTA-PSMA-GRPR complex, as evidenced by molecular docking studies that reveal a shared binding pocket between DOTA-PSMA-GRPR and PSMA-1007 (Fig. 1d), characterized by a notable overlap of their respective functional groups (Fig. 1c). Owing to the complexity of the amino acid residues involved in PSMA binding, a detailed depiction of these residues is omitted from the main text; instead, detailed interactions are provided in Fig. S12 (Supporting information). Furthermore, as illustrated in Fig. 1e, both targets of DOTA-PSMA-GRPR participate in polar interactions with the gastrin-releasing peptide receptor.

Cellular uptake and blockade studies of [^{68}Ga]Ga-DOTA-PSMA-GRPR were performed in PC3-PIP and PC-3 cells at various time points, namely 30 , 60 , 120 , and 240 min (Fig. 1f). The uptake values observed in both PC-3 and PC3-PIP cells demonstrated a positive correlation with the duration of uptake, reaching a maximum at 240 min (3.12 % ± 0.48 % for PC-3 cells and 28.43 % ± 3.69 % for PC3-PIP cells). After pretreatment with an excess of PSMA-617, the cellular uptake in PC3-PIP cells was significantly reduced at 60 min (2.45 % ± 0.33 % *vs.* 22.35 % ± 1.45 %, $P < 0.0001$), thereby emphasizing the high specificity of the probe. In the GRPR blockade group, a significant decrease in uptake was noted following pretreatment with an excess of GRPR (1.59 % ± 0.03 % *vs.* 2.17 % ± 0.21 %, $P < 0.05$). Saturation binding experiments conducted on PC3-PIP and PC3 cells revealed K_d values of 20.21 nmol/L (Fig. 1g) and 28.13 nmol/L (Fig. 1h), respectively, indicating that the probe exhibits strong affinity for both cell types.

This study involved comprehensive and detailed positron emission computed tomography (PET) imaging, the entire process of which is illustrated in Fig. 2a. The PET imaging results (Fig. 2b) indicate that [^{68}Ga]Ga-DOTA-PSMA-GRPR exhibits high targeting specificity for PC3-PIP tumor-bearing mice. Tumor uptake progressively increased from 30 min to 120 min (from 5.35 ± 0.25 %ID/g to 5.75 ± 0.05 %ID/g), whereas uptake in non-target organs, such as the kidneys and bladder, decreased rapidly, suggesting predominant renal excretion. Compared to the imaging results of [^{68}Ga]Ga-DOTA-GRPR (Fig. 2c), this probe also exhibits targeting specificity toward prostate tumors. Nonetheless, in comparison to [^{68}Ga]Ga-DOTA-PSMA-GRPR, [^{68}Ga]Ga-DOTA-GRPR demonstrated higher background radiation and a reduced target-to-non-target ratio. The imaging results for [^{68}Ga]Ga-DOTA-PSMA-617 (Fig. 2d) were comparable to those of [^{68}Ga]Ga-DOTA-GRPR, exhibiting lower background radiation but also reduced tumor uptake (5.75 ± 0.05 %ID/g *vs.* 4.05 ± 0.65 %ID/g). The results of the blocking experiments (Fig. 2e) indicated that, following PSMA-617 blockade, tumor uptake in PC3-PIP tumors was partially decreased, with a notable reduction in uptake value (from 5.35 ± 0.25 %ID/g to 1.8 ± 0.2 %ID/g). Nonetheless, due to the presence of GRPR expression, uptake was not fully inhibited. In the GRPR blocking group, the imaging results were similar to the PSMA-617 blocking experiment, with reduced tumor uptake. The results of the quantitative analysis for the organs of interest were consistent with the signal intensity changes observed in the PET images across the different groups (Figs. 2f–h). In the precursor blocking experiment, tumor uptake was completely inhibited, indicating the specificity of the probe for tumor uptake. Analysis of uptake values in vital organs of

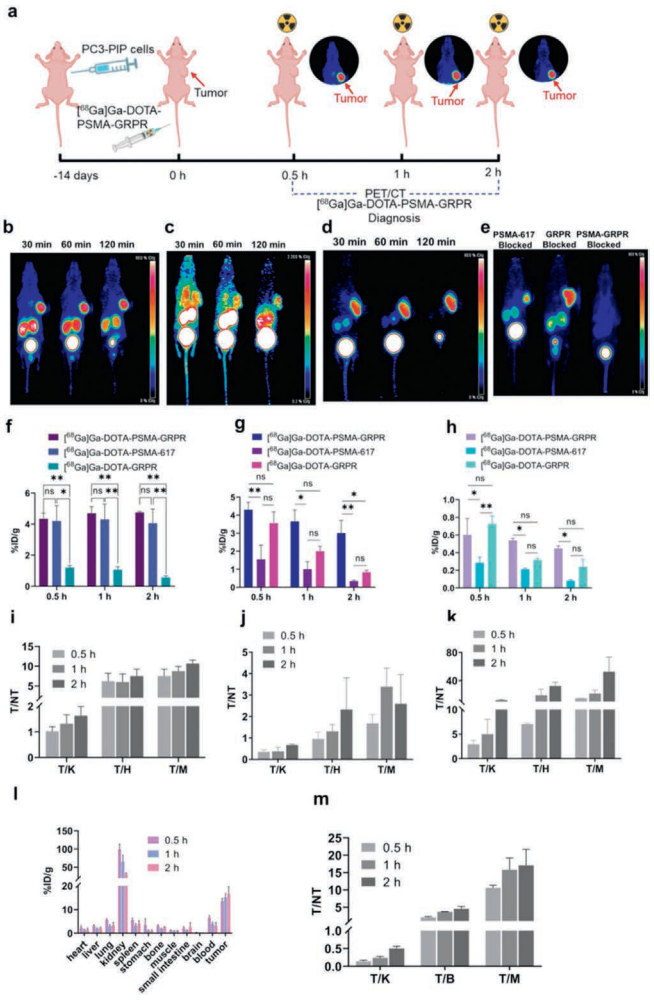


Fig. 2. Imaging, biodistribution, and data analysis in PC3-PIP tumor-bearing mice. (a) Schematic diagram of model construction and diagnosis process MIP images of mice after injection at different time points with (b) [^{68}Ga]Ga-DOTA-PSMA-GRPR, (c) [^{68}Ga]Ga-DOTA-GRPR, and (d) [^{68}Ga]Ga-DOTA-PSMA-617. (e) The blocking experiments of [^{68}Ga]Ga-DOTA-PSMA-617, [^{68}Ga]Ga-DOTA-GRPR, and [^{68}Ga]Ga-DOTA-PSMA-GRPR in mice at 30 min. Comparison of (f) tumor, (g) kidney, and (h) muscle %ID/g for three probes. PET imaging data analysis of (i) [^{68}Ga]Ga-DOTA-PSMA-GRPR, (j) [^{68}Ga]Ga DOTA-GRPR, and (k) [^{68}Ga]Ga-DOTA-MSMA-617. (l) Biodistribution results of [^{68}Ga]Ga DOTA-PSMA-GRPR at different time points in mice. (m) T/NT ratios for organs or tissues of interest (T, target tissue; NT, nontarget tissue; K, kidney; H, heart; B, blood; M, muscle). Data are presented as mean ± SD ($n = 3$). $^{*}P < 0.05$, $^{**}P < 0.01$.

tumor-bearing mice (Fig. 2i) revealed a continuous increase in the target-to-non-target organ ratio, indicating that while the probe continued to accumulate in the tumor, radioactivity in non-target organs was rapidly eliminated. Analysis of the target-to-non-target ratios in the imaging data showed that uptake in non-target organs for both [^{68}Ga]Ga-DOTA-GRPR (Fig. 2j) and [^{68}Ga]Ga-DOTA-PSMA-617 (Fig. 2k) decreased over time, with the overall target-to-non-target ratio showing an upward trend.

Furthermore, this study also investigated the biodistribution of the probe in mice bearing PC3-PIP tumors (Fig. 2l). The results indicated that the probe mainly accumulated in the kidneys and tumors, with radioactive accumulation in the kidneys rapidly decreasing over time (99.2 ± 13.85 %ID/g at 0.5 h and 32.9 ± 2.3 %ID/g at 2 h). In non-target organs/tissues, radioactive accumulation primarily occurred through renal metabolism and was rapidly excreted in urine. Conversely, radioactive uptake in tumors continuously increased over time (13.5 ± 1.2 %ID/g at 0.5 h and 16.6 ± 3.1 %ID/g at 2 h), consistent with the observations from PET images. Further analysis of the data (Fig. 2m) showed that the ratio of tumor to non-target tissues or organs increased over time, reaching a peak at 2 h.

In the PC3-PIP tumor-bearing mouse model, the present study validated the targeting capability of the [^{177}Lu]Lu-DOTA-PSMA-GRPR probe utilizing PET imaging. Subsequently, a comprehensive analysis was performed to characterize the biodistribution profile of the probe in PC3-PIP tumor-bearing mice, adhering strictly to the experimental workflow detailed in Fig. 3a. Single-photon emission computed tomography (SPECT) imaging results (Fig. 3b) revealed a high consistency between SPECT and PET images at 2 h post-injection, both of which indicated rapid clearance of radioactive material from the kidneys. By the second day post-injection, radioactive accumulation in non-target organs was nearly completely eliminated, whereas significant radioactive uptake was still observed within the tumor tissue. Importantly, a distinct radioactive signal remained detectable in the tumor on the 7th day post-injection, indicating that the [^{177}Lu]Lu-DOTA-PSMA-GRPR probe exhibits a prolonged retention time in tumor tissue, thus providing robust support for radionuclide therapy of tumors.

Furthermore, continuous monitoring of tumor volumes in various mouse models revealed that [^{177}Lu]Lu-DOTA-PSMA-GRPR, administered at different radioactive activity doses, significantly inhibited tumor growth and progression (Fig. 3c). Immunofluorescence analysis results (Fig. 3e) further demonstrated significant antitumor effects in both the high-dose and low-dose groups, whereas no such effects were observed in the saline control group, thereby confirming the outstanding antitumor properties of [^{177}Lu]Lu-DOTA-PSMA-GRPR. Additionally, no statistically significant differences were observed in body weight changes among the various mouse groups (Fig. 3d), and hematoxylin and eosin (H&E) staining of the major organs revealed no significant abnormalities (Fig. 3f), further validating the excellent biological safety of [^{177}Lu]Lu-DOTA-PSMA-GRPR.

As shown in Fig. 4a, the core innovation of this study lies in the adoption of a combined administration strategy using an ultra-low-dose radionuclide [^{177}Lu]Lu-DOTA-PSMA-GRPR and the anti-PD-1 antibody. Through the synergistic action of both agents, this approach induces a stronger tumor-specific immune response, achieving a "$1+1>2$" synergistic enhancement effect. This strategy not only significantly enhances the efficacy of tumor treatment but also ensures biosafety through dose optimization. To evaluate the therapeutic efficacy of the combined administration of an ultra-low-dose of [^{177}Lu]Lu-DOTA-PSMA-GRPR and an anti-PD-1 antibody in the treatment of tumors, we established an RM-1^{PSMA+} subcutaneous tumor mouse model in this study. Upon closely monitoring the physical status of the mice in each group, it was observed that the combined therapy of [^{177}Lu]Lu-DOTA-PSMA-GRPR and anti-PD-1 antibody demonstrated a more pronounced effect in suppressing tumor growth and arresting tumor progression, as compared to the control group and the anti-PD-1 antibody monotherapy group (Fig. 4b). Additionally, no statistically significant differences in weight changes were discerned among the diverse mouse cohorts (Fig. 4c).

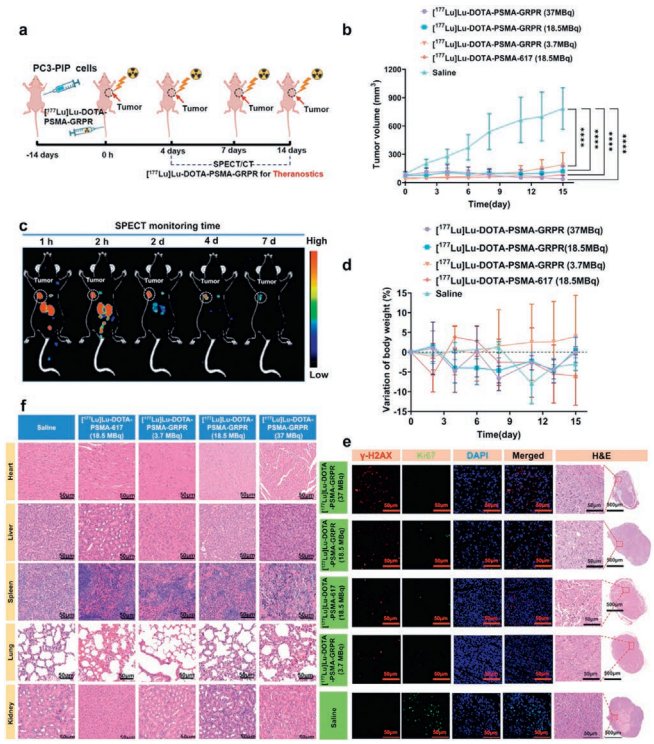


Fig. 3. [^{177}Lu]Lu-DOTA-PSMA-GRPR radionuclide therapy. A schematic diagram illustrating the construction of the PC3-PiP subcutaneous tumor model and the diagnostic and therapeutic process of [^{177}Lu]Lu-DOTA-PSMA-GRPR is presented (a). SPECT image of the high-dose group (37 MBq) of [^{177}Lu]Lu-DOTA-PSMA-GRPR-treated mice is shown (b). Monitoring curves of tumor volume (c) and body weight changes (d) in each group of mice are provided. Representative immunofluorescence staining images for 4′,6-diamidino-2-phenylindole (DAPI), Ki-67, γ-H2AX, and H&E staining of tumor tissues in each group of mice are displayed (e). Additionally, H&E staining images of vital organs in each group of mice are included (f). The mice were randomly assigned to five groups: the saline group, the [^{177}Lu]Lu-DOTA-PSMA-617 (18.5 MBq) group, the [^{177}Lu]Lu-DOTA-PSMA-GRPR (3.7 MBq) group, the [^{177}Lu]Lu-DOTA-PSMA-GRPR (18.5 MBq) group, and the [^{177}Lu]Lu-DOTA-PSMA-GRPR (37 MBq) group. Data are presented as mean ± SD ($n = 8$). $^{***}P < 0.001$, $^{****}P < 0.0001$.

Low dose radiotherapy for mouse tumors can promote T cell infiltration. The therapeutic effect depends on the mobilization of adaptive and innate immunity, as well as on cytotoxic CD4$^+$ and CD8$^+$ T cells [49]. Subsequent flow cytometry analysis disclosed that the proportion of mature dendritic cells (DCs) in the [^{177}Lu]Lu-DOTA-PSMA-GRPR + anti-PD-1 antibody combination therapy group was significantly elevated compared to the saline control group and the anti-PD-1 antibody monotherapy group (Fig. 4d). Furthermore, the infiltration of CD8$^+$ T cells in the tumor tissue was significantly greater in the combination therapy group than in the other cohorts (Fig. 4e). Moreover, a significant increase in the proportion of natural killer (NK) cells was observed in the [^{177}Lu]Lu-DOTA-PSMA-GRPR + anti-PD-1 antibody combination therapy group, as compared to the natural control group (Fig. 4f). All animal experiments were conducted in compliance with relevant national laws and regulations on animal experimentation and were approved by the Experimental Animal Ethics Committee of Xiamen University (No. XMULAC20190146).

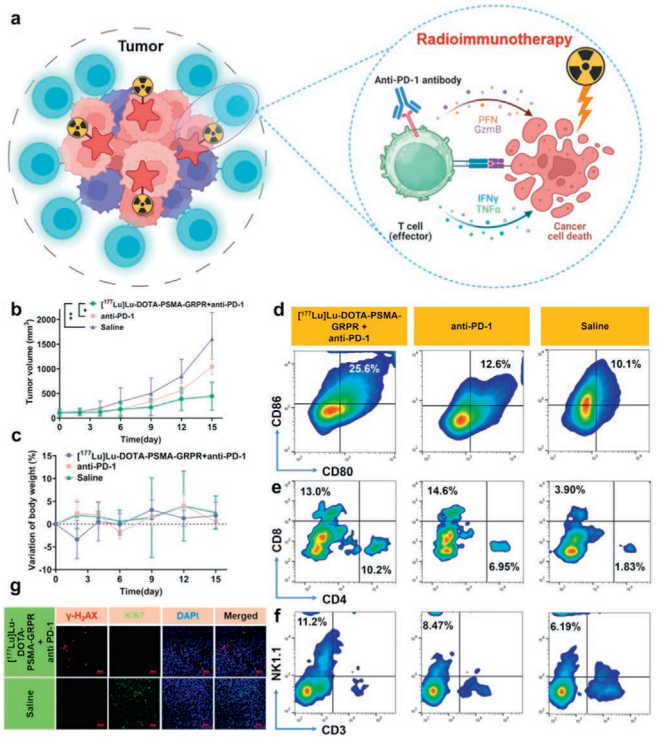


Fig. 4. Combination therapy of radiotherapy and immunotherapy in mouse subcutaneous tumor model. Mice were randomly assigned to three groups: the saline control group, the anti-PD-1 treatment group (5 mg/kg), and the combination therapy group receiving [^{177}Lu]Lu-DOTA-PSMA-GRPR (3.7 MBq) and anti-PD-1 antibody (5 mg/kg). (a) A schematic diagram depicting the mechanism of the combined therapy employing [^{177}Lu]Lu-DOTA-PSMA-GRPR and anti-PD-1 antibody in the RM-1^{PSMA+} subcutaneous tumor model. (b) Graphs illustrating the changes in tumor volume for each treatment group. (c) Charts showing the fluctuations in body weight of mice across all treatment groups. Flow cytometry analysis of tumor tissues disclosed the percentages of $CD80^+CD86^+$ dendritic cells (d), $CD3^+CD4^-CD8^+$ T cells (e), and $CD3^-NK1.1^+$ natural killer cells (f). (g) Representative micrographs showcasing DAPI, Ki-67, and γ-H2AX immunofluorescence staining, alongside H&E staining of tumor tissues and crucial organs from mice in each group. Data are presented as mean ± SD ($n = 5$). $^*P < 0.05$, $^{**}P < 0.01$.

Immunofluorescence detection further evidenced that the [^{177}Lu]Lu-DOTA-PSMA-GRPR + anti-PD-1 antibody combination therapy group displayed a high-intensity γ-H2AX signal, signifying considerable DNA damage; conversely, the saline control group exhibited a robust Ki67 signal, implying active cell proliferation (Fig. 4g). These findings provide compelling evidence for the outstanding antitumor efficacy of the combined treatment with [^{177}Lu]Lu-DOTA-PSMA-GRPR and anti-PD-1 antibody.

In summary, the combination of [^{177}Lu]Lu-DOTA-PSMA-GRPR at ultra-low doses with anti-PD-1 antibody facilitates not only the effective implementation of radionuclide therapy using [^{177}Lu]Lu-DOTA-PSMA-GRPR as a probe but also markedly activates the immune system, significantly enhancing the immune response in mice. This combined therapy cleverly integrates targeted therapeutic approaches with systemic immunomodulatory strategies, thereby exerting a positive regulatory effect on various lymphocyte subpopulations. In comparison to single high-dose radionuclide therapy or immunotherapy alone, the synergistic effect of ultra-low-dose radionuclides and immunotherapy employed in this study demonstrates more pronounced advantages in terms of enhancing the immune response of mice and improving therapeutic outcomes. This innovative and novel therapeutic strategy offers a highly promising new avenue for the treatment of numerous inoperable clinical lesions.

Declaration of competing interest

The authors declare that they have no known competing financial interests or personal relationships that could have appeared to influence the work reported in this paper.

CRediT authorship contribution statement

Hong Wang: Writing – original draft, Project administration, Methodology, Data curation. **Zhenwen Zhao:** Writing – original draft, Supervision, Methodology, Investigation, Data curation. **Xiao Xu:** Writing – review & editing, Supervision, Methodology, Funding acquisition, Conceptualization. **Zhide Guo:** Writing – review & editing, Supervision, Funding acquisition, Conceptualization. **Gang Liu:** Writing – review & editing, Supervision, Funding acquisition, Conceptualization.

Acknowledgments

This research was supported by the Guangdong Province Basic and Applied Basic Research Fund Special Project (Regional Cultivation Project) (No. 2023A1515140032) and the Open Fund of the China Spallation Neutron Source Songshan Lake Scientific City (No. KFKT2023A02).

Supplementary materials

Supplementary material associated with this article can be found, in the online version, at doi:10.1016/j.cclet.2025.111799.

References

[1] R.L. Siegel, A.N. Giaquinto, A. Jemal, *CA* Cancer J. Clin. 74 (2024) 12–49.
[2] H. Chen, F. Xu, B.B. Xu, et al., Chin. Chem. Lett. 27 (2016) 277–282.
[3] Z.X. Huang, Q. Xie, Q.P. Guo, et al., Chin. Chem. Lett. 28 (2017) 1252–1257.
[4] G. Lu-Yao, T.A. Stukel, S.L. Yao, J. Natl. Cancer Inst. 95 (2003) 1792–1797.
[5] W.H. Cooner, Invest. Radiol. 24 (1989) 257–259.
[6] J. Kurhanewicz, D. Vigneron, P. Carroll, F. Coakley, Curr. Opin. Urol. 18 (2008) 71–77.
[7] M.A. Jacobs, R. Ouwerkerk, K. Petrowski, K.J. Macura, Top. Magn. Reson. Imaging 19 (2008) 261–272.
[8] C. Barinka, P. Sácha, J. Sklenár, Protein Sci. 13 (2004) 1627–1635.
[9] R.L. Sokoloff, K.C. Norton, C.L. Gasior, K.M. Marker, L.S. Grauer, Prostate 43 (2000) 150–157.
[10] M.O. Demirkol, Ö. Acar, B. Uçar, et al., Prostate 75 (2015) 748–757.
[11] J. Deng, J. Shi, D. Li, et al., Chin. Chem. Lett. 37 (2026) 111776.
[12] S. Narayan, Y.S. Guo, C.M. Townsend, P. Singh, Cancer Res. 50 (1990) 6772–6778.
[13] H.L. Sun, Q.Y. Ma, H.G. Bian, X.M. Meng, J. Jin, Biomed. Pharmacother. 161 (2023) 114497.
[14] M. Beer, M. Montani, J. Gerhardt, et al., Prostate 72 (2012) 318–325.
[15] M. Körner, B. Waser, R. Rehmann, J.C. Reubi, Prostate 74 (2014) 217–224.
[16] H. Reile, P.E. Armatis, A.V. Schally, Prostate 25 (1994) 29–38.
[17] D.B. Cornelio, R. Roesler, G. Schwartsmann, Ann. Oncol. 18 (2007) 1457–1466.
[18] R. Mansi, X. Wang, F. Forrer, et al., Clin. Cancer Res. 15 (2009) 5240–5249.
[19] L. Baratto, H. Jadvar, A. Iagaru, Mol. Imaging Biol. 20 (2018) 501–509.
[20] M. Verhoeven, E.A.M. Ruigrok, G.J.L.H. van Leenders, et al., Front. Oncol. 13 (2023) 1199432.
[21] A. Roivainen, E. Kähkönen, P. Luoto, et al., J. Nucl. Med. 54 (2013) 867–872.
[22] E. Kähkönen, I. Jambor, J. Kemppainen, et al., Clin. Cancer Res. 19 (2013) 5434–5443.
[23] S. Mannweiler, P. Amersdorfer, S. Trajanoski, et al., Pathol. Oncol. Res. 15 (2009) 167–172.
[24] A. Iagaru, J. Nucl. Med. 58 (2017) 1883–1884.
[25] R. Minamimoto, S. Hancock, B. Schneider, et al., J. Nucl. Med. 57 (2016) 557–562.
[26] M.S. Hofman, L. Emmett, S. Sandhu, et al., Lancet 397 (2021) 797–804.
[27] O. Sartor, J. De Bono, K.N. Chi, et al., N. Engl. J. Med. 385 (2021) 1091–1103.
[28] C. Kratochwil, F.L. Giesel, M. Eder, et al., Eur. J. Nucl. Med. Mol. Imaging 42 (2015) 987–988.
[29] H. Ahmadzadehfar, K. Rahbar, S. Kürpig, et al., EJNMMI Res. 5 (2015) 114.
[30] A.S. Ravi Kumar, M.S. Hofman, J. Nucl. Med. 65 (2024) 85–86.
[31] J. Violet, S. Sandhu, A. Iravani, et al., J. Nucl. Med. 61 (2020) 857–865.
[32] P. Ma, G. Wang, K. Men, et al., Nano TransMed 3 (2024) 100036.
[33] D. De Ruysscher, G. Niedermann, N.G. Burnet, et al., Nat. Rev. Dis. Primer 5 (2019) 13.
[34] X. Wang, X. Zhong, J. Li, Z. Liu, L. Cheng, Chem. Soc. Rev. 50 (2021) 8669–8742.

[35] J. Nikitas, P. Jamshidian, A.C. Tree, et al., Lancet Oncol. 26 (2025) 378–386.
[36] J.A. Marin-Acevedo, B. Dholaria, A.E. Soyano, et al., J. Hematol. Oncol. 11 (2018) 39.
[37] N. Gavrielatou, S. Doumas, P. Economopoulou, P.G. Foukas, A. Psyrri, et al., Cancer Treat. Rev. 84 (2020) 101977.
[38] M. Zhou, S. Xiang, Y. Zhao, et al., Eur. J. Nucl. Med. Mol. Imaging 51 (2024) 369–379.
[39] S.L. Topalian, F.S. Hodi, J.R. Brahmer, et al., N. Engl. J. Med. 366 (2012) 2443–2454.
[40] J.R. Brahmer, S.S. Tykodi, L.Q.M. Chow, et al., N. Engl. J. Med. 366 (2012) 2455–2465.
[41] P. Wang, H. Zhou, G. Han, et al., World J. Surg. Oncol. 19 (2021) 205.
[42] S.F. Kammerer-Jacquet, A. Deleuze, J. Saout, et al., Int. J. Mol. Sci. 20 (2019) 1692.
[43] Z. Zeng, L. Li, J. Tao, et al., Eur. J. Nucl. Med. Mol. Imaging 51 (2024) 1221–1232.
[44] S.G. Ellsworth, et al., Adv. Radiat. Oncol. 3 (2018) 512–519.
[45] M.J. Gough, M.R. Crittenden, Neoplasia 31 (2022) 100808.
[46] J. Liu, P. Liu, J. Duan, et al., Chin. Chem. Lett. 35 (2024) 109632.
[47] M. Benešová, M. Schäfer, U. Bauder-Wüst, et al., J. Nucl. Med. 56 (2015) 914–920.
[48] O. Trott, A.J. Olson, et al., J. Comput. Chem. 31 (2010) 455–461.
[49] F.G. Herrera, C. Ronet, M. Ochoa De Olza, et al., Cancer Discov. 12 (2022) 108–133.